Paper Physics

Magdalena Kaplan*, Adam Johansson and Sören Östlund

Characterising the mechanical behaviour of dry-formed cellulose fibre materials

https://doi.org/10.1515/npprj-2024-0076 Received November 5, 2024; accepted January 3, 2025; published online January 13, 2025

Abstract: In the dry-forming process, paper pulp is formed without adding water, making it more resource-effective than traditional papermaking. It is a relatively new technology, patented only in recent years, and very few material investigations exist in the literature; hence, little is known of the constitutive behaviour. The stress state during forming is highly complex, including multiaxial loading, extreme densification, friction, large strains, and fibre-joint formation. This paper studies dry-formed materials at different compression levels, from the sparse mat to the highly densified network. Three primary loading modes are investigated: in-plane tension, out-of-plane shear and out-of-plane compression. The results indicate that the tensile modulus and strength scale quadratically and cubically to the density, respectively, while the shear properties start developing after the density passes a threshold value. The compressive properties proved difficult to quantify, mainly because of the discrepancy between the density before and after the compressive test. The dry-formed material was compared to wet-formed paper materials in the literature. This showed that the in-plane (tensile) properties and the out-of-plane shear strength are visibly lower while the shear stiffness is similar, compared to wet-formed materials. Nonetheless, the findings set a starting point for numerical simulations of the dry-forming process.

Keywords: dry-forming; fibre network density; in-plane tension; out-of-plane compression; out-of-plane shear

1 Introduction

Water is crucial in producing cellulose fibre products, such as paper, board, and miscellaneous packaging products, or so it has been believed to be for an extended time (Delgado-Fornué et al. 2011). The dry-forming process successfully forms complex, three-dimensional, and sturdy structures without addition of process water to the paper pulp (Freville et al. 2024). Fibres are instead dispersed in air, creating a sparse fibre mat or fluff (Wilson 2010) and formed under heat and pressure to reach desired shapes; see Figure 1 for reference. The technology was studied already by the end of the last century (Askling et al. 1998; Byrd 1974; Byrd 1982), but it is still considered a novel approach, given the lack of available products on the market. The technology results in a more resource-effective alternative to wet moulding, which requires considerably more energy and time to form and completely dry the product (Semple et al. 2022). The intended applications for the dry-formed products are mainly directed at replacing rigid plastic packaging. For example: trays and bowls for single use and takeaway meals, refill inserts or packaging in the beauty and cosmetics industry or inserts and lids for consumer products and electronics packaging.

Despite successful forming operations through dry forming, the low water content in the cellulose network will significantly affect the properties of the formed material. Several sources highlight the importance of water in forming the fibre-joints, which make up the network's cohesiveness (Browning 1969; Hubbe 2006; Weise et al. 1996). Water plays a significant role in phenomena occurring during network consolidation. Capillary forces will take effect upon water removal and pull the fibres closer together, facilitating molecular interactions and bonding (Hirn and Schennach 2017; Wågberg and Annergren 1997). Furthermore, water also causes the fibres to swell and creates a gel at the fibre surface (Campbell 1934; Pelton 1993) making the fibre surface softer and promoting molecular contact (Hirn and Schennach 2017). For example, Barzyk et al. (1997) enhanced the joint strength by adding carboxylic acid groups. The investigation concluded that the increase in the relative bonded area did not cause this effect; instead, it was a

^{*}Corresponding author: Magdalena Kaplan, Material and Structural Mechanics, Department of Engineering Mechanics, KTH Royal Institute of Technology, 100 44 Stockholm, Sweden, E-mail: mkaplan@kth.se Adam Johansson, Yangi AB, Honungsgatan 4b, 432 48, Varberg, Sweden Sören Östlund, Material and Structural Mechanics, Department of Engineering Mechanics, KTH Royal Institute of Technology, 100 44 Stockholm, Sweden

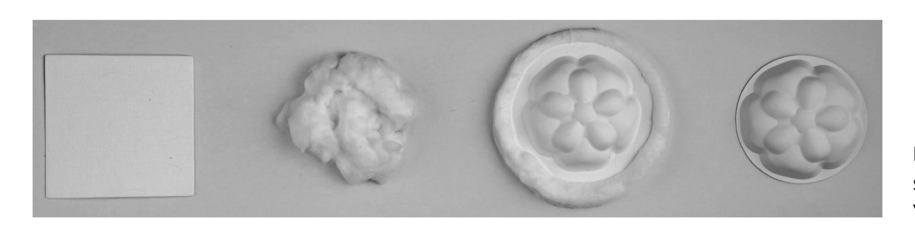


Figure 1: The stages of production of 3Dshapes through dry-forming as developed by Yangi™.

localised swelling at the surface, causing an increase in intermolecular entanglement.

Without water, the formed joints will be weaker, and the material will behave differently compared to conventional papers or wet-formed counterparts. The question that arises is how this difference is manifested. Byrd (1974) demonstrated that both density and tensile stiffness increase for increased moisture up to roughly 50 % moisture content (before pressing). Moreover, the tensile strength increases approximately linearly with moisture. Decades later, Kim et al. (2018a) confirmed the synergy between moisture and tensile strength. A few studies also investigate strength additives with the aim of improving performance. Askling et al. (1998) increased the friction in the network by adding calcium carbonate particles and cationic surface-active agents, which improved the performance. Similarly, Kim et al. (2018b) improved the tensile strength and stiffness by spraying cationic polyacrylamide and oxidised starch onto the dry network before pressing. A recent study by Loist et al. (2024) compared dry-formed papers made from hardwood and softwood with varying process parameters and found that the fibre separation prior to lay-up of the network is essential for network strength. Moreover, Pasquier et al. (2024) recently studied the effect of process conditions in terms of temperature and pressure on both dry- and wet-formed sheets, concluding that the dry-formed materials exhibited lower mechanical properties, despite similar density levels. Nonetheless, a complete understanding of the material; its limitations, and the possibilities require further characterisation.

An important aspect of material characterisation is to understand the application of interest. In this case, describing the behaviour will be useful in further developing the process as numerical simulations can replace costly prototype studies. By replicating the forming operations numerically; testing of new shapes, conditions, or even raw materials can aid in identifying potential problems and optimising the process before manufacturing. Simulations of this kind for other paper-forming processes already exist in the literature. Didone et al. (2020) developed a multiphysics model of the thermoforming process of wet-moulded pulp, which successfully replicated experimental results. Lindberg and Kulachenko (2022a, 2022b) investigated the failure behaviour of two paperboards and were able to reproduce the trayforming process numerically. The two investigated boards

were of the same type but produced in different board machines, underlining the importance of accurate material characterisation to achieve a reliable model. Like in other press-forming procedures, the resulting stress state is complex in the dry-forming process, including combinations of multiaxial loading in compression, shear, and tension (Tjahjanto et al. 2015). Therefore, these loading modes are of particular interest when performing mechanical tests where the results will be applied in forming simulations.

This paper presents a comprehensive material characterisation of dry-formed cellulose materials. The loading modes considered are in-plane tension, out-of-plane compression, and out-of-plane shear. These tests evaluate the material's performance at various densities, ranging from sparse uncompressed networks to highly densified sheets. To the best of the authors' knowledge, no previous investigations of the relation between network density and mechanical performance of dry-formed cellulose materials exist in the literature. The proposed relations between mechanical properties and density development present a first step towards formulating a numerical model.

2 Materials and methods

This section describes material selection and preparation, characterisation, specimen preparation and testing procedures for each loading mode. Before characterisation and testing, the materials were conditioned at standard climate (50 % RH, 23 °C) for at least 24 h according to ISO 187:2022. In cases where the materials had to be tested outside of a climatecontrolled environment, they were individually stored in airtight plastic bags and opened only to mount the specimen in the machine and execute the test. Based on previous observations by Linvill and Östlund (2014) and Marin et al. (2020), it is assumed that the few minutes this process took would not substantially impact the material properties, as the time frame was too short to cause significant changes in moisture.

2.1 Material selection and preparation

The fibre source used in this investigation was a softwood kraft fluff pulp produced in Sweden. During the forming process, the material will undergo drastic density changes, so the range of tested material densities spans from very sparse webs to highly compressed, dense sheets. When testing the material at different densities, the relation between density and material properties can be defined. The intermediate densities were chosen based on previous experience to reflect the various stages the material goes through during the forming process. Pads of air-laid webs were created and then compressed in a heated press under varying conditions to reach the desired densities. The exact process conditions are not disclosed here due to commercial interests; however, the forming process was in principle the same for all density levels but with varying pressure and temperature. Table 1 summarises the investigated materials, labelled as either sparse, intermediate, or dense. The labels are used to refer to the materials further on, and the three groups are, to some extent, characterised using different methods and have differing specimen geometry, as explained in the following sections.

2.2 Material characterisation

The prepared sheets were cut into specimens with dimensions specified according to the individual test modes, see Section 2.3. Next, each sample was weighed using a scale with an accuracy of 0.1 mg. The thickness was measured in two ways, depending on the type of material. For highly compressed materials (around 600 kg m⁻³ and upward), the thickness was measured according to SCAN-P 88:01 using the STFI structural thickness gauge (TJT Teknik, Sweden), which measures the thickness over a continuous line under the application of pressure between two probes, one on each side of the specimen. The method is, therefore, unsuitable for sparser materials, which were measured differently, as described below. The thickness gauge gives a continuous measurement with an interval of 0.1 mm and an accuracy of $1\,\mu m$ over the specimen strip. The measurement data was

Table 1: Summary of the tested materials.

	Material ID	Approximate density [kg m ⁻³]
Sparse	Dens65	65
	Dens85	85
Intermediate	Dens90	90
	Dens190	190
	Dens550	550
Dense	Dens930	930
	Dens1100	1,100

then used to determine an average thickness, discarding the irregularities at the edges. For the sparser materials (around 300 kg m⁻³ and downward), the measurement would significantly compress the material, because of the low stiffness in the thickness direction, resulting in a severely underestimated thickness. Instead, those materials were measured using a digital indicator with a gauge stand (Mitutoyo, Japan) with an accuracy of 1 µm. In order to avoid compressing the material locally at the gauge position, a thin glass plate was inserted between the gauge and the specimen to distribute the load. The mass of the glass plate (<5 g) was assumed to be negligible compared to the force exerted by the gauge. Three locations were measured for each specimen, from which an average thickness was determined. The in-plane area for each specimen was quantified using a digital calliper (Scala, Germany) with a 10 µm accuracy. The grammage (weight divided by in-plane area) and density (grammage divided by thickness) were then determined.

2.3 Mechanical testing

This section covers the three mechanical tests in detail. Specimens were cut to different sizes, depending on the test mode, using a punch (for the sparse and intermediate materials) or a paper guillotine (for the dense materials). Table 2 summarises the specimen dimensions for each test.

2.3.1 In-plane tension

Tensile testing of the materials was conducted according to ISO 1924-2:2008. However, the edges of the sparse materials were severely compressed upon specimen cutting, and the width of those specimens was 30 mm instead of 15 mm (see Table 2) to reduce the impact of edge effects. Additionally, the sparse specimens were reinforced with tape at the clamping edges. By slightly compressing the materials this way, mounting them in the rig was easier and prevented them from failing at the clamps. All specimens had a test length of 100 mm (the rest of the specimen length was reserved for clamping) and were uniaxially strained using a

Table 2: Summary of specimen geometries for the three testing modes.

Network	Specimen size: width \times length [mm \times mm]					
density	In-plane	Out-of-plane	Out-of-plane			
	tension	compression	shear			
$(\lesssim 100 \text{ kg m}^{-3})$	30 × 140	40 × 40	25 × 70			
$(\gtrsim 150 \text{ kg m}^{-3})$	15 × 140	40 × 40	25 × 70			

ZwickRoell tensile testing machine with a 1 kN load cell. The test setup is illustrated in Figure 2. The recorded force and deformation were then translated to stress-strain curves.

2.3.2 Out-of-plane shear

The out-of-plane shear response was measured using the rigid blocks shear setup (Nygårds et al. 2007). The specimens were cut into strips 25 mm wide and 70 mm long and then positioned between two blocks in a specially designed rig. The blocks were 19 mm wide and narrower than the specimens. The extra specimen width aided moisture absorption to the material during conditioning, but it was cut away before mounting it in the test rig. The final setup of the test is illustrated in Figure 3. To adhere the samples to the blocks, they were put in between two ColorMount dry-mount tissue strips of equal size as the specimen. The blocks containing the specimen-laminate sandwich were then put under compressive load to facilitate adhesion and heated in an oven at a target temperature of 102 °C for 2 h to melt the adhesive. The specimens were then left to cool down and condition at the standard climate for at least 24 h, after which the excess amount was cut from the blocks with a scalpel. The lamination procedure significantly decreased the thickness of the sparse materials, which is why the thickness measurement was repeated after lamination. The thickness of the blocks and the specimen-laminate sandwich was approximately measured using a digital calliper, and the specimen thickness could then be determined by subtracting the known thicknesses of the blocks and dry mount tissue. The specimens were then tested until failure in a tensile machine (MTS Systems) with a displacement rate of 0.1 mm/s while recording the displacement using an axial extensometer with a 25 mm gauge length (MTS Systems). The recorded force was translated to stress by dividing by the in-plane specimen area, and the measured displacement was converted to shear strain through division by the thickness of the specimen (measured after lamination).

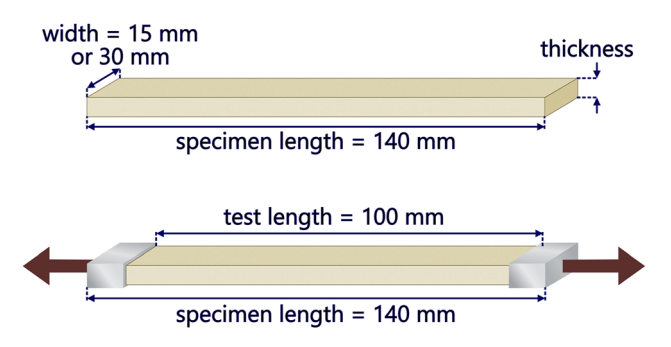


Figure 2: Setup of in-plane tensile test.

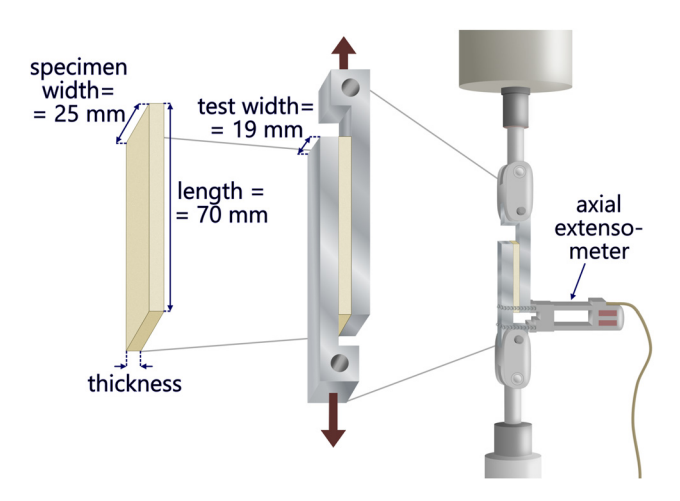


Figure 3: Setup of the out-of-plane shear test (rigid blocks shear).

2.3.3 Out-of-plane compression

The out-of-plane compression tests were conducted on quadratic specimens with a side length of 40 mm. The samples were compressed to a force of 100 kN and then unloaded. The test setup is illustrated in Figure 4. The displacement rate applied was 0.005, 0.05, or 0.5 mm/s to investigate possible rate dependence. The machine's compliance was accounted for by pressing a stiff block with approximately the same area as the samples while recording the force-displacement response, and then subtracting the machine displacement from the actual results. When calculating the strain endured by the sample, the level of zero strain was assigned at the point where the compressive stress reached 50 kPa. For the sparse materials especially, the deformation in the unpressed fibres and loose fibre ends at the highly heterogeneous surfaces might contribute to the recorded deformation. Still, it does not affect the load-bearing capacity, so a level of compressive stress above zero was used. The value was chosen by comparing the thickness recorded by the machine and the thickness of some of the samples (measured before the compression test), after which 50 kPa was found to be a

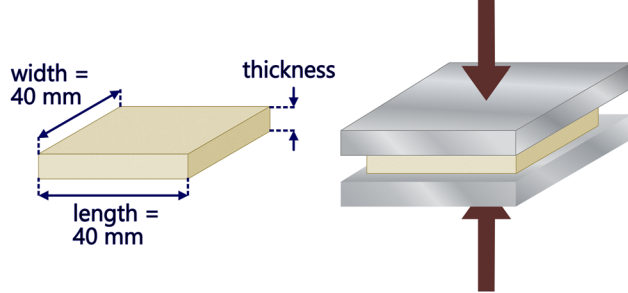


Figure 4: Setup of the out-of-plane compression test.

suitable level. For the sparse samples, the in-plane area (as well as the load-bearing area) changed significantly during the test and thus had to be remeasured. As before, the rectangular specimens' length and width were measured using a digital calliper. This area was used to determine the stress exerted on each respective specimen, and it was also used to re-evaluate the density of the samples after the compression test was finished.

2.3.4 Mean curve determination and data smoothing

A mean curve was desirable for each test mode to summarise the stress-strain behaviour. In essence, it is the average curve as seen over all specimens. Because of the low levels of both force and displacement in the out-of-plane shear test and the displacement in the out-of-plane compression test, short wavelength noise in those signals needed to be removed. After transforming displacement and force to strain and stress, both signals were smoothed using a Gaussian filter. The filter was applied using the built-in Matlab-function *smoothdata* with different window sizes depending on the test mode; the displacement in the compression test was filtered with a

window size of 10, while both displacement and force in the shear test were filtered with a window size of 100. The data was then resampled for the shear measurements to achieve an even step size in strain.

After that, the mechanical properties of each test specimen were determined: the modulus/stiffness was evaluated differently depending on the test mode. For the in-plane tensile test, the elastic modulus was determined by fitting a fifthdegree polynomial to the data and finding the maximum slope or inflexion point. The strain data was then corrected by assuming that the curve behaves linearly up to the inflexion point, thus removing the effect of any initial slack in the specimen. For the out-of-plane shear test, the shear modulus was determined by fitting a linear polynomial to a small portion of the curve, typically 5–25 % of the maximum stress. The strain data was then corrected by finding the intersection with the horizontal strain axis, $\varepsilon^{\text{corr}}$, and setting that point as the origin (zero strain). See Figure 5 (a) for a graphical representation of the strain correction. For the out-of-plane compression test, the stiffness in compression was evaluated at unloading by fitting a linear polynomial to a small portion of the data after the peak stress (from 90 to 80 % of the maximum

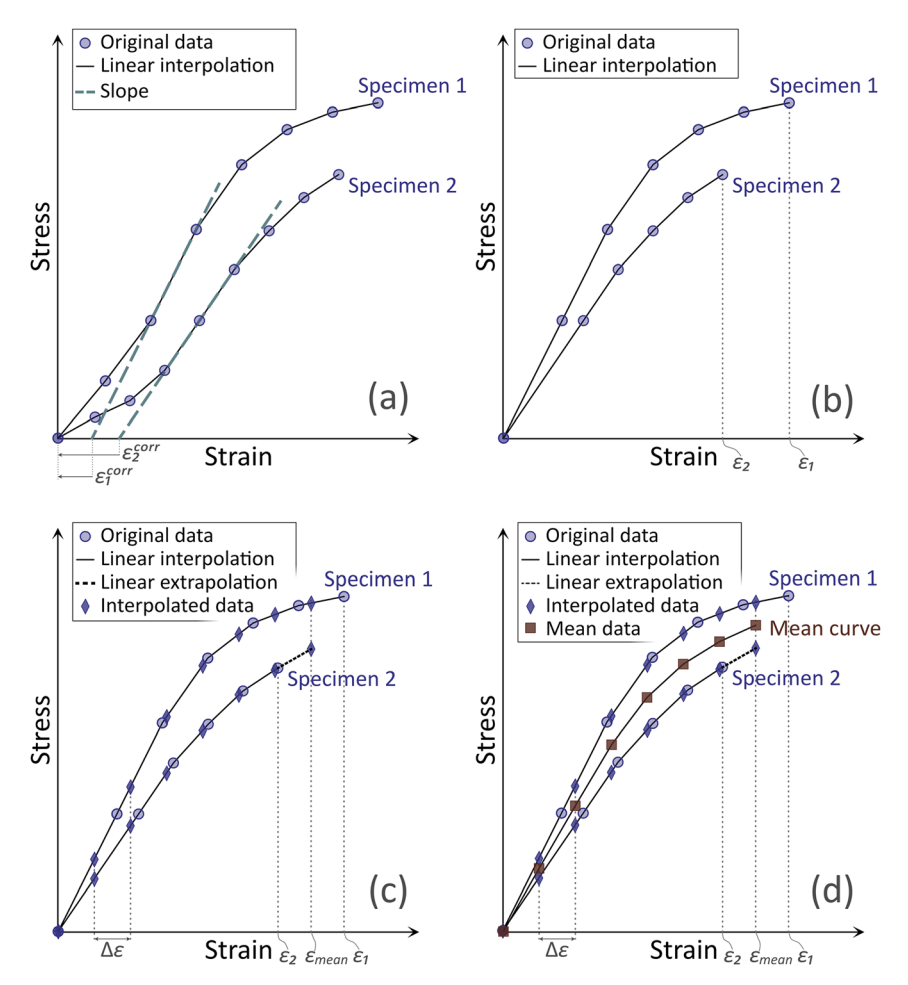


Figure 5: Schematic of the (a) zero strain correction and (b)–(d) mean curve determination: (b) the original data points of two measurements are linearly interpolated, (c) the curves are resampled up to the average strain $\varepsilon_{\text{mean}}$ with a step size of $\delta \varepsilon$, (d) the mean data is determined by averaging over the stress values.

load and down 10 data points, which corresponds to a stress range of roughly 6 MPa). When applicable, the strength was evaluated for the respective test mode and specimen as the maximum force endured by the sample, divided by the initial cross-section area. Consequently, the corresponding strain at break, was determined as the strain value corresponding to the data point of highest stress. For each test mode and density level, the individual specimens were compared by calculating the standard score based on the modulus/stiffness and, if applicable, strength. Specimens with a score higher than two were filtered out as outliers.

Mean curves were determined for the tests performed in in-plane tension and out-of-plane shear. As explained further in the Results, the discrepancy in strain for the out-of-plane compression test made it difficult to quantify a mean curve. Instead, a representative specimen curve was chosen. For the determination of mean curves, the data points were resampled using linear interpolation, as shown in Figure 5 (b)–(d). First, the data points of each specimen were linearly interpolated, see Figure 5 (b). The data was then resampled in strain for the (in-plane) tensile and (out-of-plane) shear tests. Then, the interval of resampling was determined by calculating the average maximum value of the strain

$$\varepsilon_{\text{mean}} = \frac{\sum_{i=1}^{n} \max{(\varepsilon_i)}}{n},$$
 (1)

where n is the number of considered specimens. Each specimen was then resampled with a step length of

$$\Delta \varepsilon = \frac{\varepsilon_{\text{mean}}}{N},\tag{2}$$

where N is the predetermined number of elements in the resampled vector. Figure 5 (c) shows an example of resampling the data in strain; the resampled strain vector is the same for all specimens, while the stress values are determined using linear interpolation between the original data points. For values outside of the original data range, the values were linearly extrapolated with preserved slope, see the fictive Specimen two in Figure 5 (c). Finally, the interpolated stress values were averaged over all specimens (excluding any outliers), as shown in the schematic in

Figure 5 (d). Note that the mean curves are only determined up to the maximum stress, excluding the softening behaviour after peak load, as the stochasticity of the post-peak behaviour makes it difficult to average.

3 Results

Examples of the produced materials are shown in Figure 6 in the thickness direction, demonstrating the densification of the materials.

The results from the material characterisation are shown in Figure 7. The properties were determined as previously described, and the average for each specimen was accounted for when the average for the sheet was calculated. The error bars show the spread by indicating the standard deviation, as compared between specimens. The results show that the grammage is roughly the same for all density levels (see Figure 7 (a)) and a quickly deteriorating thickness with density increase (see Figure 7 (b)). Consequently, dividing the different density groups is quite clear (see Figure 7 (c)). It is also interesting to note that the spread in grammage (shown here by the standard deviation) is comparable for the different density levels (see Figure 7 (a)), while the thickness measurement scatters significantly more for the lowest densities (<100 kg m⁻³) (see Figure 7 (b)). However, this is insignificant for the density estimation, where the spread is again small for the low-density levels (see Figure 7 (c)).

Figure 8 shows the mean curves for the in-plane tensile tests, determined and corrected as previously described in Section 2.3.4. It should be mentioned that the zero-strain correction (see Section 2.3.4 and Figure 5(a)) is applied to all presented curves. As the range of densities is large, the effect will be different on the different curves; especially for the lowest densities, the strain at break might be underreported, as low-density materials experience large fibre rotations within the network, manifested as considerable deformation at low force levels. However, the objective of this work was to systematically determine comparable properties, and the stiffness and strength will not be affected. For clarity, it

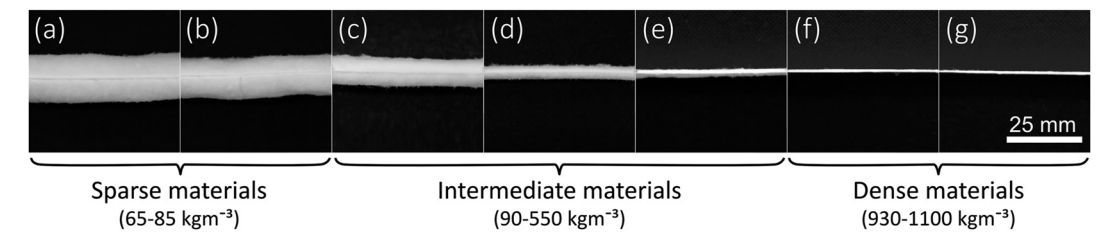


Figure 6: Density evolution of the produced materials – (a) Dens65, (b) Dens85, (c) Dens90, (d) Dens190, (e) Dens550, (f) Dens930, and (g) Dens1100. The materials' labels are presented according to Table 1.

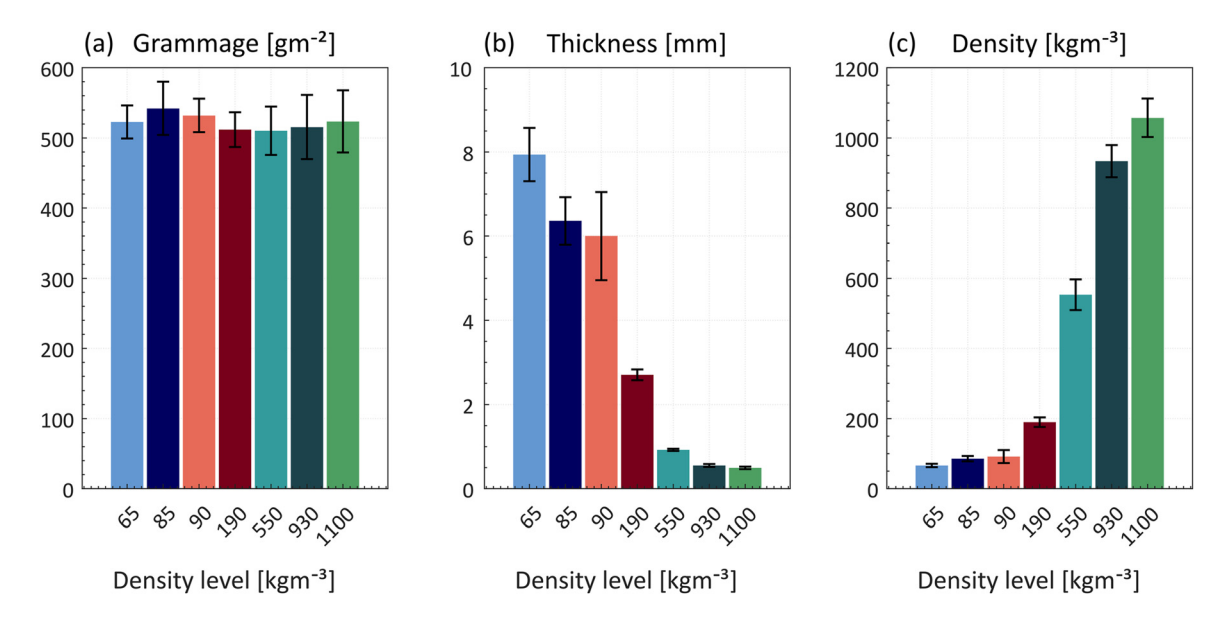


Figure 7: Characterisation of the materials showing average (a) thickness, (b) grammage, and (c) density, with error bars showing one standard deviation.

should also be noted that all curves, including the individual specimen curves, show the behaviour only up to the maximum stress, i.e. the post-peak behaviour is excluded. The curves show a clear division of the material at different density levels where the maximum stress increases with increased density. At the three highest densities, there seems to be an increase in strain as well (see Figure 8 (a)); however, at the three lowest densities, the strain at break is distinctly higher (see Figure 8 (c)).

Figure 9 shows the mean curves for the out-of-plane shear tests, determined and corrected as previously described in Section 2.3.4. The two highest densities are distinguished by higher stress values (see Figure 9 (a)) and the values drop with decreased density. However, the trend is unclear for the four lowest densities (see Figure 9 (b)). The two lowest densities also seem to endure the highest strains. The underlying specimen curves illustrate that the spread in data is large for all density levels. The spread is accounted for when

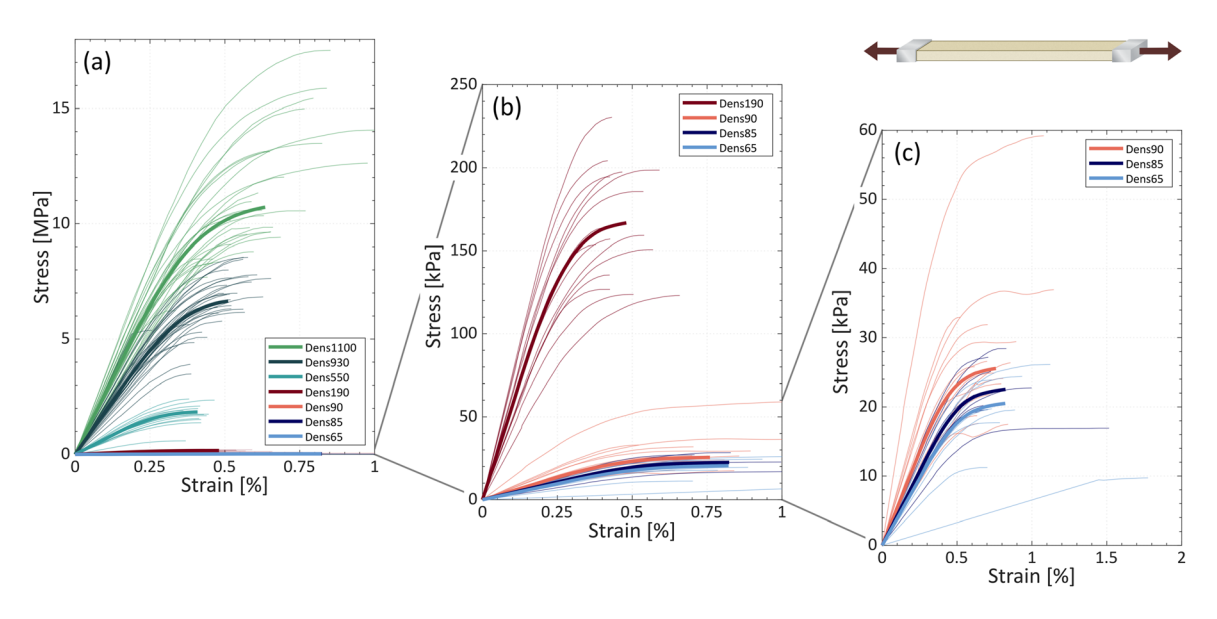


Figure 8: Stress-strain curves for the tensile tests, plotted to show all density levels: (a) the highest, (b) intermediate, and (c) lowest densities. The thick lines present the mean curve for each density level, while the thinner lines with the same colour show the curves for each individual specimen. Note the difference in scales on both horizontal and vertical axes.

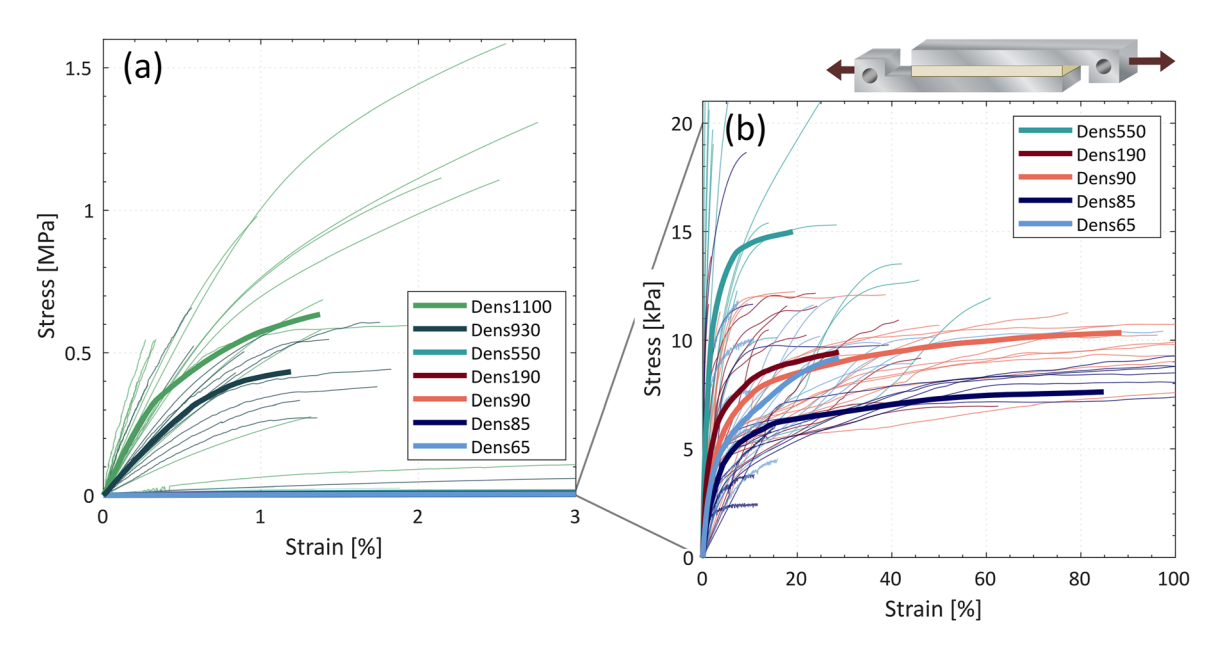


Figure 9: Stress-strain curves for the rigid blocks shear test, plotted to show all density levels: (a) the highest and (b) the intermediate and the lowest densities. The thick lines present the mean curve for each density level, while the thinner lines with the same colour show the curves for each individual specimen. Note the difference in scales on both horizontal and vertical axes.

presenting material properties later by including the standard deviation for each of the values.

Figure 10 shows the stress-strain curves for the out-ofplane compression tests. Only the two highest and the two lowest densities have been tested. All three different testing rates (0.005, 0.05 and 0.5 mm/s) are included in the measurements, but no consistent differences were found, which is why the various rates are not distinguished. As mentioned previously, the zero-deformation point was set at the compressive stress 50 kPa. However, as seen in Figure 10, the discrepancy in strain for the two dense materials is high, while the two sparse materials require significant deformation before the stress starts rising. Because of the disparity in strain, mean curves proved challenging to determine. Instead, one representative curve for each density level has been highlighted. The chosen curves lie approximately in the middle of the curves' strain span. Comparison of the different densities shows that the two lowest densities deform significantly more than the highly densified ones. The spread in strain is, however, greater for the highly densified materials. No limit load could be found for any of the tested materials, i.e. no reduction in stress due to material degradation was observed during the test. The flattening of the curves close to the peak load is caused by the machine approaching its allowed applied force. After peak load, the unloading curve is also included. These initial slope at unloading is then used to determine the stiffness in compression, which is discussed further in the section Analysis and discussion. Also, it should be noted

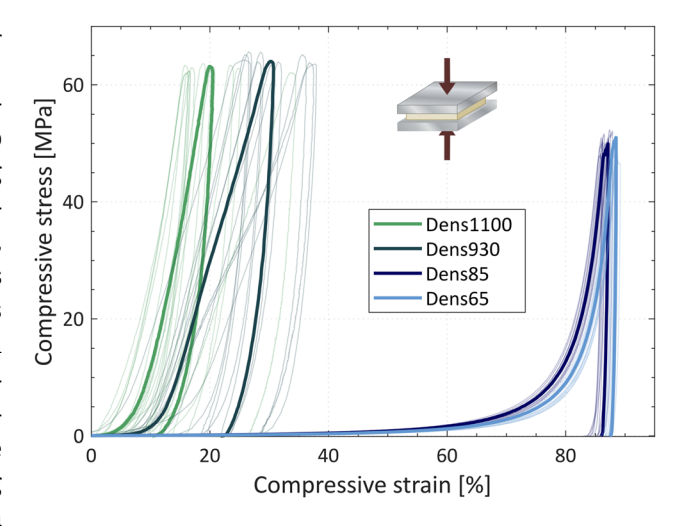


Figure 10: Stress-strain curves for the compression tests. The thick lines present a representative curve for each density level, while the thinner lines with the same colour show the curves for each individual specimen. The flattening of the curves close to the peak load is caused by the machine approaching its allowed applied force.

that the individual curves exhibit spring-back recovery. However, this was not further analysed here.

4 Analysis and discussion

Mechanical properties can be extracted from the mean curves shown in Figures 8–10 in the Results section. The

mechanical properties were evaluated at each density level for each loading mode. In all three test modes, the initial, linear stiffness of the material can be described by the tensile modulus, shear modulus, and the stiffness in compression. Strength and strain at break are also reported for the tensile and shear tests. In the case of the compression tests, no reduction in force was recorded despite load levels up to ~60 MPa, see Figure 10, consequently, only the stiffness is reported. The procedure for determining the mechanical properties is described in Section 2.3.4.

4.1 In-plane tension

As seen in Figure 11 (a), the tensile modulus and strength trends are similar. In both cases, the values are extremely low for the lowest densities, but they start increasing immediately as the density increases. The increase is slow in the beginning and rapid by the end. The increasing trend is expected for two reasons. First, when the thickness of the material decreases (density increases), the stress of the material will increase because of the decreased crosssectional area, even if the load-bearing capacity of the material remains the same. If this were to account for all of the strength increase, the recorded force would be constant across density levels and the tensile properties proportional to their respective density levels. The second reason is that increased density facilitates fibre-joint formation, increasing the load-bearing capacity of the network. Among others, Toll (1998) showed that there exists a proportionality between the volume fraction of fibres and the number of fibre intersections. With an increased number of joints, loads can be more efficiently distributed among fibres, and the endured force increases, so the tensile properties develop faster than the density increases. This aligns with previous findings by Deogekar et al. (2019), where the strength of stochastic fibre networks was numerically shown to depend on the joint density rather than the network density.

It should also be mentioned that the different specimen widths (see Table 2 and Figure 2) might have an influence on the strength of the material, as a larger volume increases the probability of failure (Hagman and Nygårds 2012). However, this effect is considered to be small. The width is higher for the two lowest densities, which show an extremely low strength. Even an increase in strength as high as 100 % would not notably affect the shape of the strength curve shown in Figure 11 (a). Further, the variability in the lowest densities is very high, as seen in the strain at break in Figure 11 (b); the spread in data is thus likely greater than the effect of the specimen width.

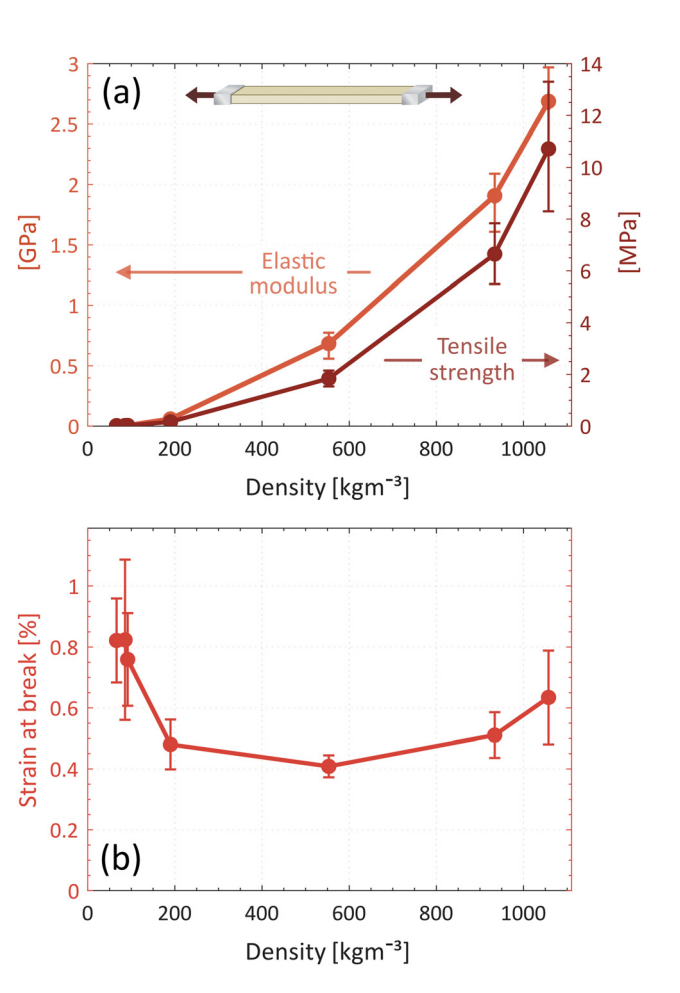


Figure 11: Average tensile properties from uniaxial tensile tests: (a) modulus and strength, and (b) strain at break. The error bars indicate the standard deviation within each density level.

Figure 11 (b) shows the development of the strain at break over the investigated densities. At first glance, it looks as if it is quite high at the lowest densities, then rapidly decreases, and finally slightly recovers at the end. In reality, the changes in the strain are quite small, and the high value in the beginning can likely be attributed to the lack of consolidation between fibres, allowing fibres to move freely and inducing high degree of rotations in the sparse networks, as is shown in Figure 12 (a). The embrittlement of the network upon density increase aligns with previous numerical findings (Deogekar and Picu 2018). However, considering the spread within each density level, it is difficult to establish a clear trend for the strain at break in uniaxial tension.

Table 3 compares the determined tensile properties with a few wet-formed materials from the literature. The values are reported for a highly densified board with a grammage of 120 g cm⁻¹, tested in both the machine and cross directions (Tryding 1996), a thermoformed material of bleached kraft pulp aimed for replacing beverage carton

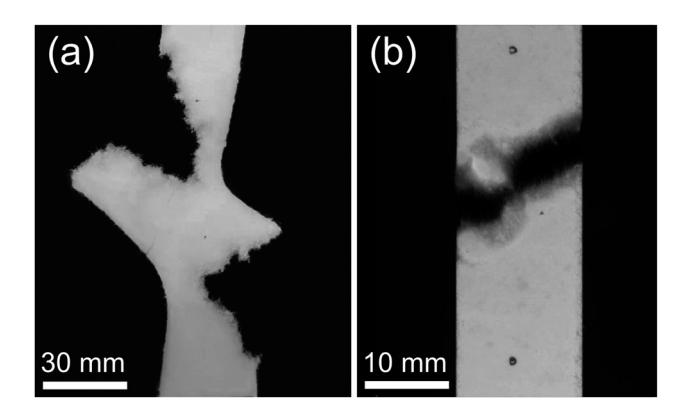


Figure 12: Examples of fractured tensile specimens, showing (a) the rotation in the network of a sparse material, and (b) the straighter crack profile of a dense material. Note that the two images have different scales.

cups (Chinga-Carrasco et al. 2024), and a hot-pressed chemo thermomechanical pulp (CTMP) (Asta et al. 2024). In order to make a fair comparison between the materials, despite differences in grammage, the tensile stiffness index (TSI), i.e. the specific modulus, and the tensile index (TI), i.e. the specific strength, are reported. The dry-formed materials exhibit lower strength, stiffness, and strainability than the wet-formed counterparts. Interestingly, all three wetformed examples have reasonably similar stiffness and strength, but the strain at break is much higher for the board. Compared to the dry-formed samples, the strain at break is roughly 10 times higher in the board. However, the thermoformed material exhibits strains about 1.5-5 times lower than the board, about 2-4 times higher than the dryformed materials. The conclusion is that the dry-formed material does not form as strong fibre-joints because of the low moisture content during pressing, which is expected. This means that these materials could not directly replace the wet-formed materials in all applications. However,

understanding the properties needed in specific applications is vital in choosing the suitable material without overdesigning.

The failure of the tensile specimens is further analysed in Figure 12, which shows photographs of two failed specimens. As can be seen in Figure 12 (a), the crack develops at a substantial angle relative to the loading direction in the sparse specimen, indicating a high degree of rotation in the network. When the material has been densified, the crack is less skewed, and the network rotation is not visible, see Figure 12 (b). As shown previously by Deogekar and Picu (2018) network heterogeneity allows more uniform deformation, while a (more) homogenous network will develop localised damage. Consequently, heterogeneity promotes ductile failure, while homogeneity makes the network brittle. The difference in fracture mechanisms between the dense and sparse networks at hand shows the transition from a highly heterogeneous network to a more homogenous one, which in turn points to fibre-joint formation. The numerical work of Islam and Picu (2018) further supports this conclusion; by showing that increasing the number of joints per fibre will inhibit the network from re-orienting under applied loading. However, the visible fibre pull-out and apparent profile in the thickness direction (Figure 12 (b)) imply that fibre joint failure is still the primary failure mechanism.

4.2 Out-of-plane shear

As can be seen in Figure 13 (a), the development of shear modulus and strength with density is similar, with very low values in the beginning and no significant increase until the density reaches $\sim 600 \text{ kg m}^{-3}$. After this, the properties pass a threshold and increase rapidly for the two highest densities. This is in line with previous findings, for example, the relation

Table 3: Comparison of the determined in-plane tensile properties with wet-formed examples form the literature.

Material type	Density [kg m ⁻³]	Elastic modulus [GPa]	Tensile strength [MPa]	Strain at break [%]	TSI ^a [kNm g ⁻¹]	TI ^b [Nm g ⁻¹]
Dry-formed	930	1.9	6.5	0.51	2.0	7.1
Dry-formed	1,100	2.7	11	0.63	2,5	10
Board (Tryding 1996)	779	3.57-6.78 ^c	37.4-57.7 ^c	6.0-2.6 ^c	4.6-8.7 ^c	48-74 ^c
Wet-formed (thermoformed)	1,179	4.65	35.4	1.9	3.9	30
bleached kraft (Chinga-Carrasco et al. 2024)						
Wet-formed, bleached CTMP	996	8.5	58	1.2	8.53	58.1
(hot-pressed) (Asta et al. 2024)						

^aTensile stiffness index (specific modulus) ^bTensile index (specific strength) ^cThe values given in the interval represent the cross and machine directions.

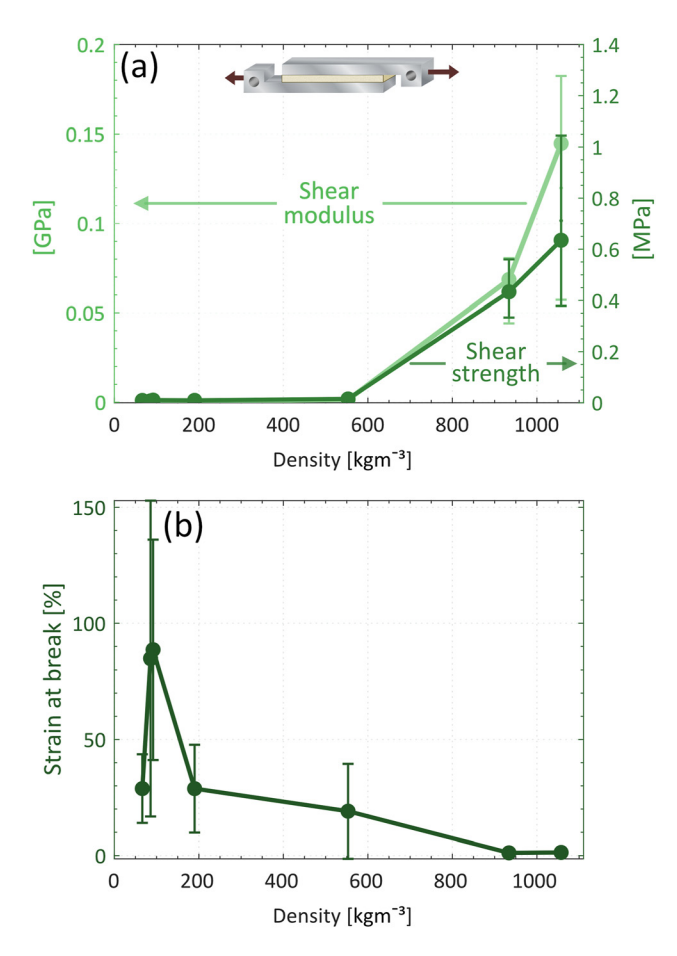


Figure 13: Shear properties from RBS-tests: (a) shear modulus and shear strength and (b) strain at break. The error bars indicate the standard deviation within each density level.

between the shear modulus G, density ρ and percolation density $\rho_{\rm th}$ as stated by Picu (2011): $G \propto (\rho - \rho_{th})^h$, (where h is reported to be a scalar in the range of 1–3). This relation will be further evaluated in Section 4.4. The abrupt behaviour

change indicates that the material transitions from an entangled network, where fibres are free to move and the movement is only limited by friction, to a cross-linked network, i.e. where fibres are connected through fibre-joints. Additionally, Pan and Carnaby (1989) showed that the shear modulus depends partly on the number of sliding contacts in the network. However, this abrupt change was not seen in the development of tensile properties (see Figure 11 (a)), which instead demonstrates a continuous increase with increased density. A possible explanation is that the friction between the entangled fibres is sufficient to give the network some resistance to the applied load in-plane, while the out-of-plane shearing mode allows the fibres to slide more freely until the fibre-joints are formed. Another possibility is that the lowdensity materials are heterogenous in the thickness direction. with a higher density at the top and bottom (at the lamination sites) and a lower density in the core. As the cross-section bears the load in the in-plane tension uniformly, it would not have an effect there, but in the out-of-plane shear, the weakest location in the thickness direction would determine the strength. This could be further investigated by inspecting the through-thickness profile of the shear specimens, which was not possible here due to induced damage during the removal of the specimens from the blocks.

The strain at break, shown in Figure 13 (b) demonstrates an unclear trend. The material with the lowest density breaks at (on average) 30 % of strain, while the remaining two sparse densities break at almost (on average) 90 % strain. However, the spread in the data at those densities is extensive. The strain measurement is susceptible to the initial thickness, as it is small compared to the applied displacement. Since the sparse specimens had to be remeasured after mounting in the blocks (see Section 2.3.2), it is possible to attribute some of the spread to the uncertainty in the measurement of the initial thickness. However, it can be safely assumed that the sparse

Table 4: Comparison of the determined out-of-plane shear properties with wet-formed examples from the literature.

Material type	Density [kg m ⁻³]	Shear modulus [MPa]	Shear strength [MPa]	Strain at break [%]	Specific shear modulus [Nm g ⁻¹]	Specific shear strength [Nm g ^{–1}]
Dry-formed	930	69	0.43	1.2	73	0.46
Dry-formed	1,100	140	0.64	1.4	140	0.60
Paperboard (Nygårds et al. 2007)	779	_	1.04-1.10 ^a	_	_	1.33-1.41 ^a
Paperboard (Nygårds and Malnory 2010)	649	_	1.1 ^{b,c}	_	-	1.7 ^{b,c}
Copy paper (Nygårds and Malnory 2010)	800	_	1.3 ^b	_	-	1.6 ^b
Westrock paperboard (Srinivasa et al. 2018)	_	84-100 ^a	1.5-1.7 ^a	2.6-3.0 ^a	-	-
BillerudKorsnäs paperboard (Srinivasa et al. 2018)	-	35-53ª	0.80-0.96 ^a	4.1–5.5 ^a	-	-

^aThe values given in the interval represent the cross and machine directions. ^bMeasured with the notched shear test (NST). ^cAverage value based on measurements at different thickness positions.

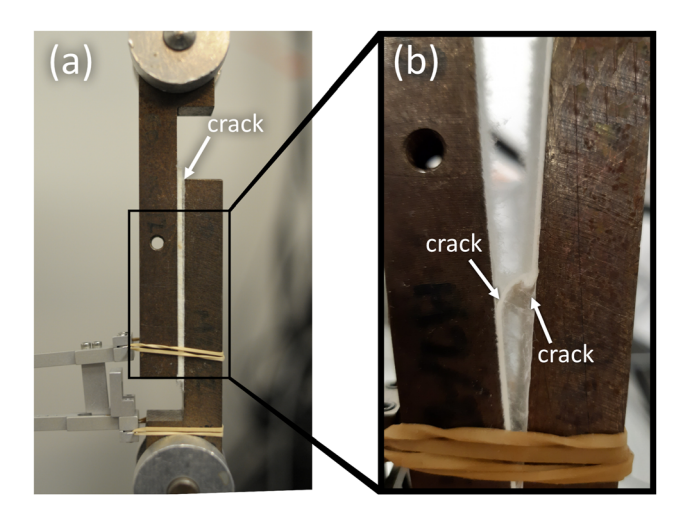


Figure 14: Examples of failed shear specimens: (a) specimen mounted in the test rig after failure, (b) close-up of the fracture after dismounting the blocks from the machine.

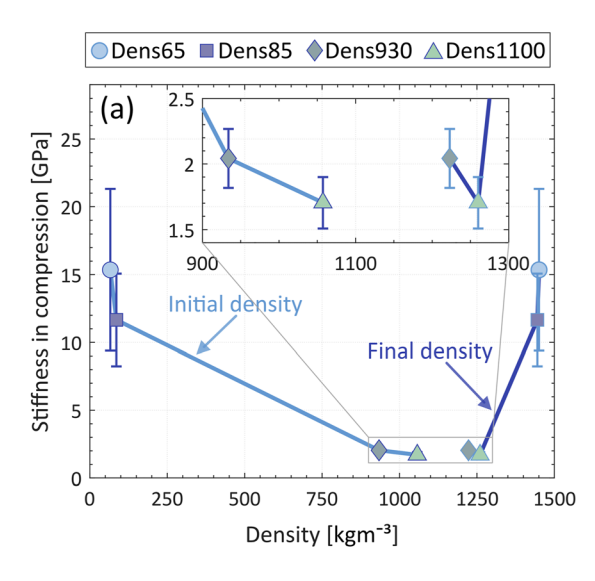
densities break (on average) at a strain of at least 30 %; the value then drops to less than 2 % at the two highest densities. This aligns with the increase in shear modulus and strength and supports the idea that fibre-joints develop after the density reaches 600 kg m^{-3} . The network becomes more constrained when the joints develop, as fibres can no longer slide freely, reducing the endured strain but increasing the load-bearing capacity. Consequently, the sparse fibre mats are more formable than the pressed sheets. The importance of fibre sliding for formability is also pointed out by Hauptmann et al. (2015).

Table 4 compares the determined shear properties with wet-formed materials from the literature. The compared materials are diverse types of paperboards measured with rigid blocks in the machine and cross directions (Nygårds et al. 2007; Srinivasa et al. 2018), and paperboard and copy paper measured using a different evaluation of the out-of-plane shear, the notched shear test (Nygårds and Malnory 2010). The dry-formed material is visibly weaker in the shear mode; however, the difference is not as dramatic as in the case of the tensile properties. Additionally, the materials are quite stiff, and even exceed the value for the shear modulus for some of the paperboards. The strain at break is comparatively lower, which is unsurprising since the dry-formed materials are quite stiff yet weak.

Figure 14 shows the typical failure of the specimen in the rigid blocks shear setup. In all cases, the material failed by developing cracks along the length of the specimen close to the top and the bottom surfaces of the sheet, see the close-up in Figure 14 (b). The dry-formed materials are subjected to

Table 5: Average densities of the tested materials in compression: before and after compression up to 100 kN ($\sim 50-60 \text{ MPa}$).

	Initial density [kg m ⁻³]	Final density [kg m ⁻³]
Sparse	66 86	1,451 1,445
Dense	933 1,057	1,223 1,260



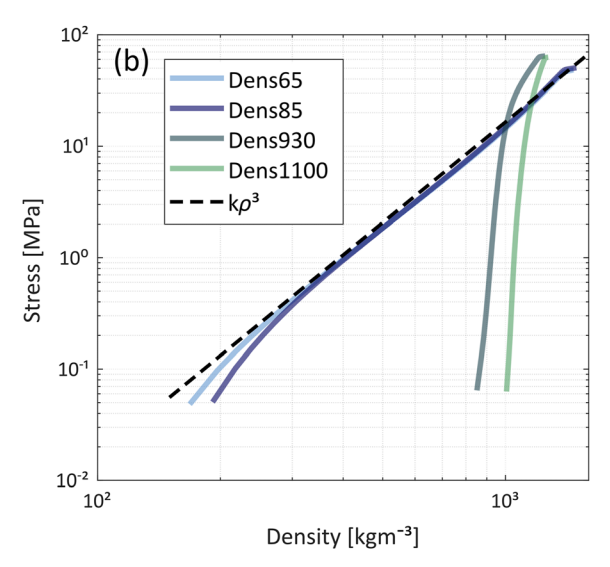


Figure 15: Analysis of compression curves: (a) average stiffness in compression versus initial density before compression (left, light blue plot) and final density at maximum compression (right, dark blue plot), and (b) stress-density curves plotted in logarithmic scale with a fitted power law curve, where $k = 16.5 \cdot 10^{-3} \text{ Nm}^7 \text{ kg}^{-3}$. Note that the high stiffness values in (a) (for the initially low-density materials) are likely an effect of the extreme level of compression and should not be interpreted as the actual material stiffness.

pressure and heat during production (at varying degrees). Since heat is applied to the surface, it is possible that fibrejoint formation is especially favoured close to the surface. Consequently, further away from the outer surfaces, in the middle plane, there are fewer constraints from the fibre joints, and the material allows for more fibre movements, resulting in larger strainability. At the surface, where the network is more restricted, failure will initiate when the deformation is large enough.

4.3 Out-of-plane compression

The curves presented in Figure 15 (a) show the development of the stiffness in compression versus initial density and the final density (the density at the moment of unloading). The final density was estimated by dividing the grammage (weight divided by the in-plane area of each specimen measured after compression) by the thickness at the maximum compression (determined from the recorded displacement in the testing machine for each specimen). The final densities determined for the materials are presented in Table 5. Notably, the initially sparse specimens have reached a much higher density than the dense ones, approaching the theoretical limit: the density of cellulose at 1,500 kg m⁻³. Islam and Picu (2018) show that a network held together by fibre-joints can be compacted less than an equivalent network without fibre-joints, since the joints restrict the fibres from moving freely and thus inhibit the network's deformation. In this case, the difference in compression of the initially sparse and dense networks proves that fibre-joints are formed during the dry-forming process. However, the final densities in the compression test for those materials are likely overestimated since they are close to the theoretical limit. One possible source of error is that the thickness is evaluated at the maximum load when the material is highly compressed, while the in-plane area is determined after unloading. Consequently, the elastic deformation due to the applied load is not accounted for in both cases, and it would have been more accurate to measure the in-plane area before unloading. However, this was not technically possible.

The curve based on the initial density shown in Figure 15 (a) demonstrates a decreasing trend with increased (initial) density. However, accounting for the final density, the second curve is more convincing, with an increasing trend with increased (final) density. The difference between the highest (~15 MPa) and lowest (~2 MPa) values is considerable. Moreover, the spread in the two high values for the two initially lowest densities is vast and makes the trend uncertain. As shown in the magnification, the difference between the two lowest values is slight. Nonetheless, the initially sparse materials show a significantly stiffer behaviour after compression. This can, yet again, be attributed to the lack of fibrejoints. The sparse materials have been compressed without the addition of external heat, while the initially dense materials have been formed (prior to the compression test) with both high pressure and heat, which is known to facilitate the formation of fibre-joints. This is supported by the results in the recent study by Pasquier et al. (2024), where the thermoforming temperature was found to be of great importance for the mechanical properties of the dry-formed material.

Figure 15 (b) shows the stress-density curves plotted in log-log scale and a curve fitted to the model proposed by van Wyk (1946), stating that the compressive stress p in a fibrous mass is proportional to the cubed density ρ ($p \propto \rho^3$). As can be seen in the resulting plot, the (initially) low-density materials follow this relation well. In contrast, the (initially) highdensity materials exhibit a vastly different behaviour (the average slope is much higher than three). The scaling constant k has thus been determined from a least-square fit to the data from both (initially) low-density curves. This result supports the previously stated findings. The (initially) lowdensity materials both behave like a mass of fibres; like nonwovens or yarns, as in the theory of van Wyk. However, the (initially) high-density materials do not follow the same relation, because they are highly consolidated networks with fibres connected through fibre joints.

A comparison between the stiffness in compression of the dense materials with values found in the literature is presented in Table 6. The dry-formed materials are compared to one type of pressboard, for which the stiffness in compression has been evaluated at different compressive

Table 6: Comparison of the determined out-of-plane stiffness in compression with wet-formed examples form the literature.

Material type	Density [kg m ⁻³]	Stiffness in compression [GPa]	Specific stiffness in compression [kNm g ⁻¹]
Dry-formed	930 ^a	2.0	2.2
Dry-formed	1,100 ^a	1.7	1.6
Pressboard (undeformed) (Tjahjanto et al. 2015)	1,100-1,250	0.40	0.36-0.32
Pressboard (compressed by ~10 %) (Tjahjanto et al. 2015)	1,100-1,250 ^a	1.23	1.1-0.98

^aInitial density before compression.

strains: 0 and 10 % (Tjahjanto et al. 2015). The comparison shows that the dry-formed materials are stiffer than the pressboard. However, it should be taken into account that the degree of compression is roughly 20–30 % (see Figure 10). which could explain why the value is higher. Moreover, it could also explain why the compression stiffness is high for the sparse materials (see Figure 15 (b)), since the compressive strain reaches up to 90 %. However, the recorded strain is difficult to interpret, especially in sparse materials. As seen in Figure 10, the compressive strain initially increases while the stress remains small despite the zero-deformation level being set above zero compressive stress. This is likely related to the high porosity in the material and deformation in the rough surface. As both Robertsson et al. (2023) and Hagman and Rydefalk (2024) showed, the initially flat part of the compressive stress-strain curve is an effect of the specimen's geometric properties. With an even more heterogeneous and porous material at hand, this effect is likely amplified for the sparse fibre mats.

As mentioned previously, no limit load could be found in the compressive test despite stress levels at $\sim\!60$ MPa. The permanent deformation is, however, significant, especially for the sparse materials, which are compressed to $\sim\!10$ % of their initial thickness (see Figure 10). This is also clearly visible in inspecting the samples before and after the compression test, see Figure 16 (a) and (b). On the other hand, the highly densified samples are not visibly deformed when comparing the samples before and after, see Figure 16 (c) and (d). A permanent deformation of roughly 20–30 % is recorded during the test, see Figure 10, which might be too small to see when inspecting the samples with the naked eye. After the compression, the previously sparse specimens bear a high resemblance to the initially highly densified sheets. The

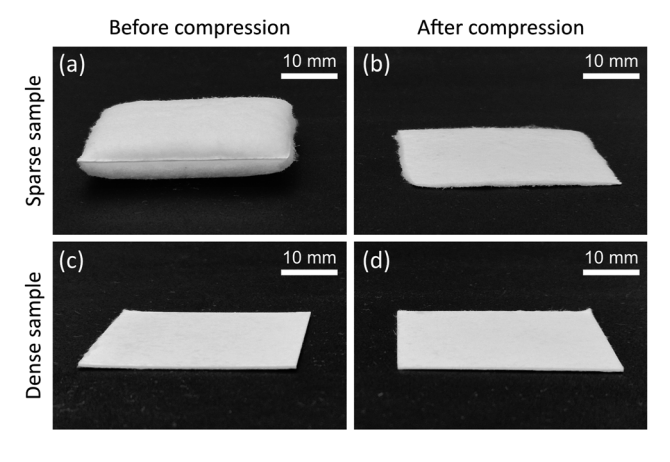


Figure 16: Compressive samples compared before and after pressing, for sparse and highly densified material: sparse sample (a) before and (b) after compression test, dense sample (c) before and (d) after compression test.

significant difference is the surface, which is not as smooth and shows free fibres sticking out. As discussed before, fibre-joints are most likely formed close to the surface during the forming process with the aid of the supplied heat. The dense samples were subjected to heat during the pressing, and since the compressive test was conducted without an external heat source, it should be the cause of the difference in the surface seen between the previously sparse samples and the initially dense ones.

4.4 Comparison between loading modes

Figure 17 shows a comparison of the evolution of properties in the in-plane tensile and out-of-plane shear modes and curves fit to the moduli and strength using a power law. The respective constant given for each curve was determined by a least square fit. As seen in Figure 17 (a) and (b), the tensile modulus and strength increase continuously, while the shear modulus and strength increase rapidly only after passing the threshold at ~600 kg m⁻³. The curve fits show that the tensile modulus E scales quadratically with the density ρ ($E \propto \rho^2$). Previous findings by Deogekar and Picu (2018) demonstrate a linear relationship between modulus and density. However, the dry-forming process affects the network in several ways. Apart from bringing the fibres close together, fibre-joints are also formed, and the fibre morphology might also be affected. Both effects are included in the density parameter here. The shear modulus G is also proportional to the density squared, after the percolation density $\rho_{\rm th}$ ($G \propto (\rho - \rho_{th})^2$), which agrees well with the previously mentioned relation from (Picu 2011): the determined exponent lies in the proposed interval of 1-3.

Further, the curve fit of the tensile strength $\sigma_{\rm max}$ shows a cubic scaling with the density $(\sigma_{\text{max}} \propto \rho^3)$, while the shear strength au_{max} scales linearly with the density after the percolation density $(\tau_{\text{max}} \propto (\rho - \rho_{\text{th}}))$. The observed threshold in shear properties at ~600 kg m⁻³ likely corresponds to a critical transition in the fibre network structure. At lower densities, the network is mainly held together by friction and entanglements. When the density increases, two factors contribute to the increase in mechanical properties: (i) increased proximity and contact between fibres and (ii) fibre-joint formation. After the threshold density, the two factors contribute to forming a network with enough cohesion to resist shear transformation, which aligns with findings in the literature (Picu 2011), as discussed before. This threshold is not seen for the tensile properties, which develop continuously and benefit even from very few formed fibre-joints. In other words, different mechanisms govern the behaviour in tension and in shear, where effective shear resistance requires a

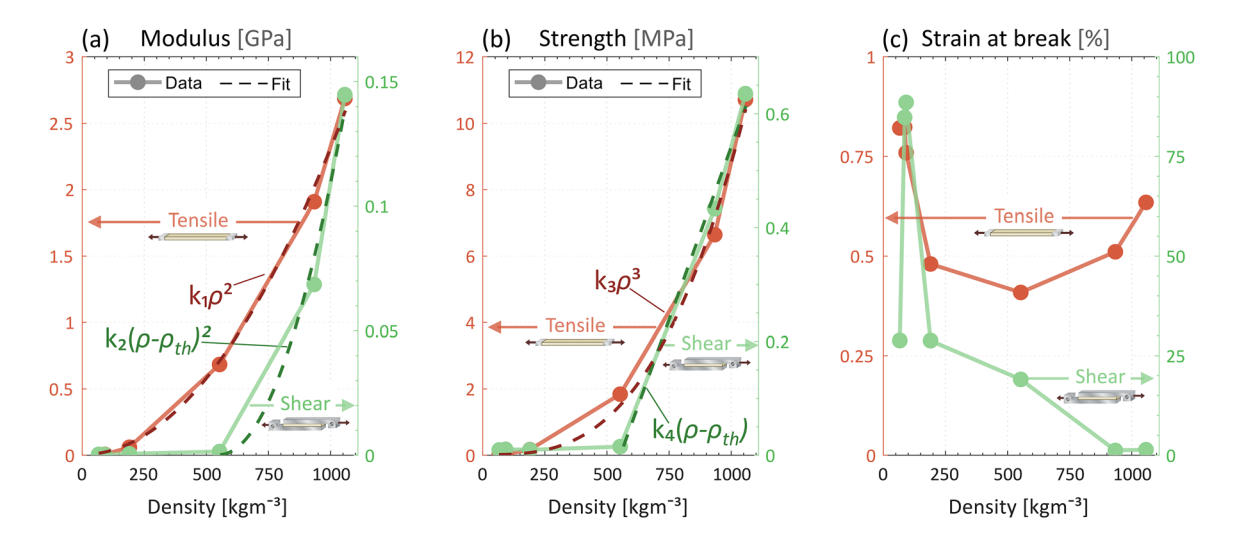


Figure 17: Average mechanical properties compared between two of the test modes: (a) modulus with fitted curves, (b) strength with fitted curves, and (c) strain at break for in-plane tension and out-of-plane shear. Note the differing scales on the vertical axes. The constants in the curves fitted to the moduli and strengths are: $k_1 = 2.32 \cdot 10^{-3} \text{ Nm}^4 \text{ kg}^{-2}$, $k_2 = 546 \text{ Nm}^4 \text{ kg}^{-2}$, $k_3 = 8.80 \cdot 10^{-3} \text{ Nm}^7 \text{ kg}^{-3}$, and $k_4 = 1.22 \cdot 10^3 \text{ Nm kg}^{-1}$. The percolation density ρ_{th} is assumed to be 553 kg m⁻³.

more comprehensive network structure, while tensile properties evolve gradually.

Figure 17 (c) compares strain at break for the tensile and shear tests. Both values start out high, but the tensile strain seems relatively stable, while the shear counterpart drops when the density increases. The initial strainability is an essential factor for the formability of the network; as previously shown by Östlund et al. (2011), both strength and deformation in the network are needed to form 3-dimensional structures successfully. Naturally, this is most important at the lowest densities as that is where the shape of the structures are formed. However, the spread in each value makes the trends less clear. The spread of the strain at break can be seen in Figure 11 (b) for the tensile mode and in Figure 13 (b) for the shear mode.

5 Conclusions

The material investigation presented in this work shows how (in-plane) tensile, (out-of-plane) shear, and (out-of-plane) compressive properties develop with increased density for dry-formed cellulose materials. The study extends the knowledge of the deformation and damage mechanisms experienced by dry-formed materials during forming. For example, the tensile tests show that fibre-joint failure is the dominating fracture mechanism, even for the densest materials (≥1,000 kg m⁻³). For the lowest densities, the networks are mainly governed by friction and fibre rotation, and consequently, these materials are quite ductile and, in extension, formable but weak.

It is found that the tensile modulus and strength quadratically and cubically with the density, respectively, while the shear counterparts only develop after a threshold is surpassed at ~600 kg m⁻³. In both cases, the strain at break is also drastically reduced with increased density, indicating a transition from a formable, yet weak, to a very brittle, but stiff and strong, material. Both of these observations align with the theory that fibre-joints develop in the material despite the low moisture content present during the consolidation of the network. However, the dry-formed materials are weaker and more brittle than the wet-formed counterparts, both in tension and shear. The in-plane (tensile) stiffness is also lower, while the out-of-plane shear modulus seems to be similar.

The compressive properties prove difficult to quantify, but the formed materials show a high stiffness when compared to values in the literature, which is attributed to a high density caused by the high degree of compaction. No load limit has been found, i.e. no reduction in load-bearing capacity has been observed despite high compressive forces. Secondly, the large spread in data at the lowest (initial) densities makes it difficult to establish a trend. However, comparison of the compressive behaviour of sparse fibre mats and highly densified sheets shows a vast difference in the behaviour of the two materials; the heat and pressure used to form the sheets hugely contribute to the consolidation of the network. In future work, investigating the material behaviour under combined compression and heat would give insight into the material's behaviour during forming, which is needed to create a reliable material model.

Nevertheless, the demonstrated relationships between material density and mechanical properties present a suitable starting point for developing a density-dependent constitutive model. In future work, the results can be applied to forming simulations for which the transitions in material behaviour are accounted for. The results will be useful for developing the dry-forming process further by replacing expensive and timeconsuming prototype studies.

Acknowledgments: The authors gratefully acknowledge the funding of the FutureForm-project, as well as the participants and collaborators within the project. The authors would also like to acknowledge Prashanth Srinivasa, Anton Hagman, Gustav Marin, and Cecilia Rydefalk at RISE Bioeconomy for support in the experimental procedures.

Research ethics: Not applicable. Informed consent: Not applicable.

Author contributions: The authors have accepted responsibility for the entire content of this manuscript and approved its submission. MK, AJ, and SÖ formulated the problem statement together. MK and SÖ decided on the testing methods. AJ developed the forming process and produced the materials. MK carried out the mechanical tests, analysed the data, created the visualisations, and wrote the initial draft, which AJ and SÖ both reviewed. SÖ acquired the

Use of Large Language Models, AI and Machine Learning Tools: None declared.

Conflict of interest: Adam Johansson is employed by Yangi AB. All other authors state no conflict of interest.

Research funding: The project Design of future proof biobased packaging for increased circularity (FutureForm) has been funded by the Strategic Innovation Programme Bio-Innovation with support from Vinnova, Swedish Energy Agency, and FORMAS.

Data availability: The raw data can be obtained on request from the corresponding author.

References

- Askling, C., Wågberg, L., and Rigdahl, M. (1998). The effect of additives on the mechanical properties of dry-formed fibre networks. J. Mater. Sci. 33: 1997-2003, https://doi.org/10.1023/A:1004390313084.
- Asta, N., Kaplan, M., Kulachenko, A., Östlund, S., and Wågberg, L. (2024). Influence of density and chemical additives on paper mechanical properties. Cellulose 31: 5809-5822, https://doi.org/10.1007/s10570-024-05917-6.
- Barzyk, D., Page, D.H., and Ragauskas, A. (1997) Carboxylic acid groups and fibre bonding. In: Baker, C.F. (Ed.). Trans. of the XIth fund. Res. Symp. Cambridge, 1997. Fundamental Research Committee (FRC), Manchester, pp. 893-907.

- Browning, B.L. (1969). The nature of paper. In: Proceedings of the thirtyfourth annual conference of the graduate library school. The University of Chicago Press, pp. 18-38.
- Byrd, V.L. (1974). How much moisture is needed to develop strength in dryformed handsheets? Tappi J. 57: 131-133.
- Byrd, V.L. (1982). Bonding of-air laid webs Critical amount of moisture necessary. Tappi J. 65: 153-155.
- Campbell, W.B. (1934). Hydration and beating of cellulose pulps. UTC, Montreal. Chinga-Carrasco, G., Ruwoldt, J., Pasquier, E., Dalheim, M.Ø., and Wieser, M.K. (2024). Development of a beverage carton closure cap based on 100% wood pulp fibres. J. Clean. Prod. 445: 141339, https:// doi.org/10.1016/j.jclepro.2024.141339.
- Delgado-Fornué, E., Contreras, H.J., Toriz, G., and Allan, G.G. (2011). Adhesion between cellulosic fibers in paper. J. Adhes. Sci. Technol. 25: 597-614, https://doi.org/10.1163/016942410X530951.
- Deogekar, S. and Picu, R.C. (2018). On the strength of random fiber networks. J. Mech. Phys. Solids 116: 1–16, https://doi.org/10.1016/j.jmps. 2018.03.026.
- Deogekar, S., Islam, M.R., and Picu, R.C. (2019). Parameters controlling the strength of stochastic fibrous materials. Int. J. Solids Struct. 168: 194-202, https://doi.org/10.1016/j.ijsolstr.2019.03.033.
- Didone, M., Mohanty, S., Hattel, J.H., Sonne, M.R., Fiordaliso, E.M., Checchi, A., and Tosello, G. (2020). On the drying process of molded pulp products: experiments and numerical modelling. Dry Technol. 38: 1644-1662, https://doi.org/10.1080/07373937.2019.1653905.
- Freville, E., Pescheux-Sergienko, J., Mujica, R., Rey, C., and Bras, J. (2024). Novel technologies for producing tridimensional cellulosic materials for packaging: a review. Carbohydr. Polym. 342: 122413, https://doi. org/10.1016/j.carbpol.2024.122413.
- Hagman, A. and Nygårds, M. (2012). Investigation of sample-size effects on in-plane tensile testing of paperboard. Nord. Pulp Paper Res. J. 27: 295-304, https://doi.org/10.3183/npprj-2012-27-02-p295-304.
- Hagman, A. and Rydefalk, C. (2024). Z-directional testing of paperboard in combined tensile and compression loading. Tappi J. 23: 268-284, https://doi.org/10.32964/TJ23.5.268.
- Hauptmann, M., Wallmeier, M., Erhard, K., Zelm, R., and Maischak, I.-P. (2015). The role of material composition, fiber properties and deformation mechanisms in the deep drawing of paperboard. Cellulose 22: 3377-3395, https://doi.org/10.1007/s10570-015-0732-x.
- Hirn, U. and Schennach, R. (2017) Fiber-fiber bond formation and failure: mechanisms and analytical techniques. In: Batchelor, W., and Söderberg, D. (Eds.). Trans. Of the XVIth fund. Res. Symp. Oxford, 2017. Fundamental Research Committee (FRC), Manchester, Oxford, pp. 839-863.
- Hubbe, M.A. (2006). Bonding between cellulosic fibers in the absence and presence of dry-strength agents - a review. Bioresources 1: 281-318, https://doi.org/10.15376/biores.1.2.281-318.
- Islam, M.R. and Picu, R.C. (2018). Effect of network architecture on the mechanical behavior of random fiber networks. J. Appl. Mech, Trans. ASME 85, https://doi.org/10.1115/1.4040245/422743.
- Kim, J.-M., Hwang, M.-G., Oh, K., Jung Youn, H., and Lee, H.-L. (2018a). How can we improve strength property of dry formed papers? Appita: technology, innovation. Manuf., Environ. 71: 58-65, https://doi.org/10.3316/informit.
- Kim, J.W., Kim, J.M., Oh, K., and Lee, H.L. (2018b). Strength improvement of dry formed paper by spraying of dry strength agent and hot pressing. Appita: technology, innovation. Manuf., Environ. 71: 66-71.
- Lindberg, G. and Kulachenko, A. (2022a). The effect of ply properties in paperboard converting operations: a way to increase formability. Cellulose 29: 6865-6887, https://doi.org/10.1007/s10570-022-04673-9.

- Lindberg, G. and Kulachenko, A. (2022b). Tray forming operation of paperboard: a case study using implicit finite element analysis. Packag. Technol. Sci. 35: 183-198, https://doi.org/10.1002/pts.2619.
- Linvill, E. and Östlund, S. (2014). The combined effects of moisture and temperature on the mechanical response of paper. Exp. Mech. 54: 1329-1341, https://doi.org/10.1007/s11340-014-9898-7.
- Loist, M., Kleinert, R., Miletzky, F., and Schreiber, S. (2024). Comparison of bleached hardwood and softwood kraft dry pulps for semi-dry papermaking with different dry forming processes. Holztechnologie 2: 32 - 37
- Marin, G., Nygårds, M., and Östlund, S. (2020). Stiffness and strength properties of five paperboards and their moisture dependency. *Tappi* /. 19: 71-85, https://doi.org/10.32964/TJ19.2.71.
- Nygårds, M. and Malnory, J. (2010). Paper physics: measuring the out-ofplane shear strength profiles in different paper qualities. Nord. Pulp Paper Res. J. 25: 366-371, https://doi.org/10.3183/npprj-2010-25-03p366-371.
- Nygårds, M., Fellers, C., and Östlund, S. (2007). Measuring out-of-plane shear properties of paperboard. J. Pulp Pap. Sci. 33: 105–109.
- Östlund, M., Borodulina, S., and Östlund, S. (2011). Influence of paperboard structure and processing conditions on forming of complex paperboard structures. Packag. Technol. Sci. 24: 331-341, https://doi.org/10.1002/pts.
- Pan, N. and Carnaby, G.A. (1989). Theory of the shear deformation of fibrous assemblies. Text. Res. J. 59: 285-292, https://doi.org/10.1177/ 004051758905900506.
- Pasquier, E., Mörseburg, K., Syverud, K., and Ruwoldt, J. (2024). Effect of raw material and process conditions during the dry forming of CTMP fibers for molded pulp products. J. Nat. Fibers 21, https://doi.org/10.1080/ 15440478.2024.2409890.
- Pelton, R. (1993). A model of the external surface of wood pulp fibers. Nord. Pulp Paper Res. J. 8: 113-119, https://doi.org/10.3183/npprj-1993-08-01p113-119.

- Picu, R.C. (2011). Mechanics of random fiber networks a review. Soft Matter 7: 6768, https://doi.org/10.1039/c1sm05022b.
- Robertsson, K., Engqvist, J., Wallin, M., Ristinmaa, M., Tryding, J., and Borgqvist, E. (2023). Out-of-plane uniaxial loading of paperboard: experimental procedure and evaluation. Nord. Pulp Paper Res. J. 38: 389-398, https://doi.org/10.1515/npprj-2023-0017.
- Semple, K.E., Zhou, C., Rojas, O.I., Nkeuwa, W.N., and Dai, C. (2022). Moulded pulp fibers for disposable food packaging: a state-of-the-art review. Food Packag. Shelf Life 33: 100908, https://doi.org/10.1016/j. fpsl.2022.100908.
- Srinivasa, P., Sundström, J., and Nygårds, M. (2018). Shear mechanics: evaluation of paperboard and liner shear properties using rigid block shear test method. RISE Bioeconomy report number: 9. Unpublished.
- Tjahjanto, D.D., Girlanda, O., and Östlund, S. (2015). Anisotropic viscoelastic-viscoplastic continuum model for high-density cellulosebased materials. J. Mech. Phys. Solids 84: 1-20, https://doi.org/10.1016/ j.jmps.2015.07.002.
- Toll, S. (1998). Packing mechanics of fiber reinforcements. Polym. Eng. Sci. 38: 1337-1350, https://doi.org/10.1002/pen.10304.
- Tryding, J. (1996). Plane fracture of paper. Lund University, Lund. van Wyk, C.M. (1946). Note on the compressibility of wool. J. Text. Inst. Trans. 37: T285-T292, https://doi.org/10.1080/ 19447024608659279.
- Wågberg, L. and Annergren, G. (1997). Physicochemical characterization of papermaking fibres. In: Baker, C.F. (Ed.). Trans. of the XIth fund. Res. Symp. Cambridge, 1997. Fundamental Research Committee (FRC), Manchester, pp. 1-82.
- Weise, U., Maloney, T., and Paulapuro, H. (1996). Quantification of water in different states of interaction with wood pulp fibres. Cellulose 3: 189-202, https://doi.org/10.1007/BF02228801.
- Wilson, A. (2010). 1 The formation of dry, wet, spunlaid and other types of nonwovens. Applications of Nonwovens in Technical Textiles 3-17, https://doi.org/10.1533/9781845699741.1.3.